https://doi.org/10.5194/egusphere-2026-3096
Preprint. Discussion started: 10 June 2026

Effectiveness of olivine dissolution in beach simulations for ocean alkalinity enhancement – insights from flow-through experiments

Sonja Geilert[1], Lucille Hoogerdijk[1], Yasmina Ben Hammou Abboud[1], Fabrice Pernet[2], Jessica Volz[1], Andre Baldermann[3], Mariëtte Wolthers[1], Cale A. Miller[1]

[1]Department of Earth Sciences, Geosciences, Utrecht University, Utrecht, The Netherlands
[2]Ifremer, Université de Brest, CNRS, IRD, LEMAR, F-29840 Argenton, France
[3]Institute of Applied Geosciences, Graz University of Technology and NAWI Graz Geocenter, Graz, Austria

Corresponding author: Sonja Geilert (s.geilert@uu.nl)

Abstract

Carbon Dioxide Removal (CDR) is required to mitigate climate change and to keep global warming below 1.5 to 2°C. Ocean alkalinity enhancement (OAE) in the coastal environment is a promising and relatively low-cost technique, that could enhance marine CO_2 sequestration via silicate weathering. The high-energy environment in the surf zone is especially promising as constant grain collision provides a natural grinding mechanism, potentially enhancing alkaline mineral dissolution. In this study, we experimentally investigated the dissolution of dunite, an olivine-rich ultramafic rock, in natural Atlantic seawater using flow-through reactors. In the experiment, pure dunite (from now on referred to as olivine; forsterite endmember), beach sand (from the coast of West Brittany) and a mixture of olivine and beach sand (olivine/sand) was studied under turbulent and stagnant conditions, in order to identify the effect of grinding on mineral dissolution and alkalinity generation. We see, that alkalinity release was highest in all turbulent reactors compared to stagnant conditions, with the highest alkalinity release observed in the turbulent olivine/sand mixture (11.5 mmol mol^{-1} olivine d^{-1}). The effective sand grinding and especially the hardness of the quartz grains, composing 49 wt.% of the sand, enhance olivine abrasion and rounding, and thus foster dissolution. This effect diminishes over experimental time, when an apparent steady state is reached after ca. 74 hours, where a constant alkalinity release from the turbulent olivine/sand treatment is attained with 1.1±0.6 mmol mol^{-1} olivine d^{-1}; within error to turbulent treatments of pure olivine (1.0±0.2 mmol mol^{-1} olivine d^{-1}). With respect to potentially toxic trace metals (Ni, Cr), we observe high concentrations in the first 24 hours for the olivine/sand treatment when mineral dissolution rates were high (Ni: 359 nmol L^{-1}; Cr: 171 nmol L^{-1}), but these decrease quickly to background seawater values (Ni: 18 nmol L^{-1}; Cr: 19 nmol L^{-1}). In addition, our results show that the natural alkalinity release from sand was not diminished by olivine addition, and that the probability of secondary mineral precipitation and by this CO_2 release is mostly low, due to high dilution rates with ambient seawater. A cooperative alkalinity release by sand and olivine is expected in natural conditions where similar high dilution rates of reaction products will prevail. Our study shows that ephemeral peaks of high critical element (e.g. Ni) concentrations due to high mineral reaction rates in the beginning of the experiment can be avoided, thus, olivine addition to surf zones could be an efficient marine CDR technique for OAE applications in coastal environments.

https://doi.org/10.5194/egusphere-2026-3096
Preprint. Discussion started: 10 June 2026

1. Introduction

Climate change mitigation measures include the aim to limit global warming to between 1.5 and 2°C, by drastic reduction of greenhouse gas emissions and additional atmospheric Carbon Dioxide Removal (CDR) (IPPC, 2023). Marine CDR (mCDR) receives special attention as the ocean is one of the largest sinks of atmospheric CO_2 and takes up about one third of anthropogenic CO_2 emissions (Friedlingstein et al., 2025). Ocean Alkalinity Enhancement (OAE) via the addition of alkaline minerals and rocks in the coastal area is a promising technique with high CO_2-sequestration potential (Eisaman et al., 2023; Oschlies et al., 2023). The increase in total alkalinity (TA) via mineral dissolution increases the buffer capacity of the ocean and enhances the reservoir of dissolved inorganic carbon (DIC) in the form of bicarbonate and carbonate ions on timescales greater than 10000 years (Middelburg et al., 2020). Forsterite, the Mg-endmember of olivine minerals, is considered a suitable mineral due to its high CO_2-sequestration potential, global availability and relatively fast dissolution rates. In theory, 1 mol of forsterite can sequester 4 mols of CO_2 via the idealized reaction:

$$Mg_2SiO_4 + 4CO_2 + 4H_2O \rightarrow 2Mg^{2+} + H_4SiO_4 + 4HCO_3^- \quad \text{Eq. 1}$$

However, in practice, this idealized CO_2-sequestration is often impacted by secondary reactions, such as carbonate or phyllosilicate precipitation, and/or incomplete olivine dissolution (Griffioen, 2017; Fuhr et al., 2022; Moras et al., 2022; Geerts et al., 2025; Miller and Pernet, 2025).

The coastal environment can be divided into a high- and low-energy environment, representing the surf zone at beaches and the shelf area, respectively (Meysman and Montserrat, 2017; Eisaman et al., 2023). Both environments offer specific advantages considering mineral dissolution in the OAE context, that is a natural grinding mechanism in the surf zone and micro- and macrofauna enhanced dissolution by metabolic reactions in the low-energy benthic environment (Meysman and Montserrat, 2017; Geerts et al., 2025). Experimental investigations of both OAE-settings show high potential concerning TA increase and modelling studies related CO_2-sequestration, however, exact quantification of the alkalinity increase remains challenging due to natural TA fluxes from sediments (Fuhr et al., 2023, 2024; Bach, 2024; Ramasamy et al., 2024; England and Bach, 2025).

Beach applications provide several advantages, which include good accessibility and high wave energy, facilitating a natural grinding and abrasion mechanism via mineral collision with sand grains. This sand-collision effect results in faster mineral dissolution and the physical modification of grain size creating a higher surface area-to-volume ratio (Oelkers et al., 2018). This natural grinding mechanism could save energy and costs on mineral treatment before OAE applications. The effectiveness of grain collision on olivine dissolution in the OAE context has already been shown in experiments (Flipkens et al., 2023; Bach, 2024; England and Bach, 2025), however, these experiments were conducted in batch reactors, likely showing a faster alkalinity build-up compared to the open ocean with high dilution caused by mixing and lateral transport from surrounding seawater. In addition, several challenges remain with respect to the potential of coastal applications, that are (1) the impact on natural alkalinity release from sand (Bach, 2024; England and Bach, 2025), (2) the release of trace (potentially toxic) metals to the marine ecosystem (Montserrat et al., 2017; Fuhr et al., 2022; Flipkens et al., 2023), and (3) the risk of secondary mineral formation that could reduce the net CO_2-sequestration capacity (Fuhr et al., 2022; Moras et al., 2022; Suitner et al., 2024). In addition, mineral reactivity decreases with time, due to the potential formation of passivating surface layers, for example, by the precipitation of (metal-bearing) amorphous SiO_2 layers (Béarat et al., 2006; Oelkers et al., 2018), though the abrasion effects in the surf zone may counter this.

https://doi.org/10.5194/egusphere-2026-3096
Preprint. Discussion started: 10 June 2026

In our study, we conducted stagnant and turbulent flow-through experiments, simulating olivine addition to the surf zone where high dilution factors with ambient seawater would occur. This setup allowed us to assess the alkalinity build-up due to grain collision and examine if trace metal concentrations higher than background values were reached. Further, we discuss the attainment of saturation states for secondary precipitates and assess the suitability of OAE to mitigate climate change in high-energy coastal environments.

2. Material and methods

2.1. Experimental set-up

As flow-through reactors, Artemio® Set incubation cones (JBL) have been used with the purpose to simulate mineral addition to high-energy beach settings. The reactors were filled with 600 ml of natural coastal seawater UV treated and filtered at 5 µm pumped into the Ifremer (Institut Français de Recherche pour l'Exploitation de la Mer) experimental laboratory (Argenton, France, 48° 31.2768' N, -4° 46.1016' W) at the start of the experiment. The incoming seawater came from a pool, which is renewed with each spring tide, filtered at 1µm, and UV-treated before being delivered to the reactors (Di Poi et al., 2022). The reactors were then continuously flushed with filtered seawater at a flow rate of 80 – 100 ml hr^{-1}. At the reactor outlet, the seawater was filtered through a 50 µm mesh in order to avoid the loss of fine-grained particles. Solid material consisted of dunite, with 88% of the grains between 0.355 and 0.710 mm in size (the remaining 12% were between 0.250 and <0.063mm) provided from the company Sibelco™, mined in Årheim, Norway. This dunite was composed of 75% Mg-olivine (endmember forsterite); from here on referred to as olivine. Beach sand was collected outside the experimental laboratory in Argenton and was sieved to 0.5 mm in order to match the average grain size of the olivine and autoclaved to remove organics. All reactors were filled with a total of 11 g solid material composed of either (1) olivine, (2) beach sand or (3) olivine/sand (2.2 and 8.8 g, respectively). Each treatment was conducted in triplicates and performed under stagnant and turbulent conditions, summing up to 18 reactors in total (Fig. 1). Turbulent conditions in 9 reactors—simulating grain collision from wave action— were created by bubbling with high-flow air from the bottom (Fig. 1).

https://doi.org/10.5194/egusphere-2026-3096
Preprint. Discussion started: 10 June 2026

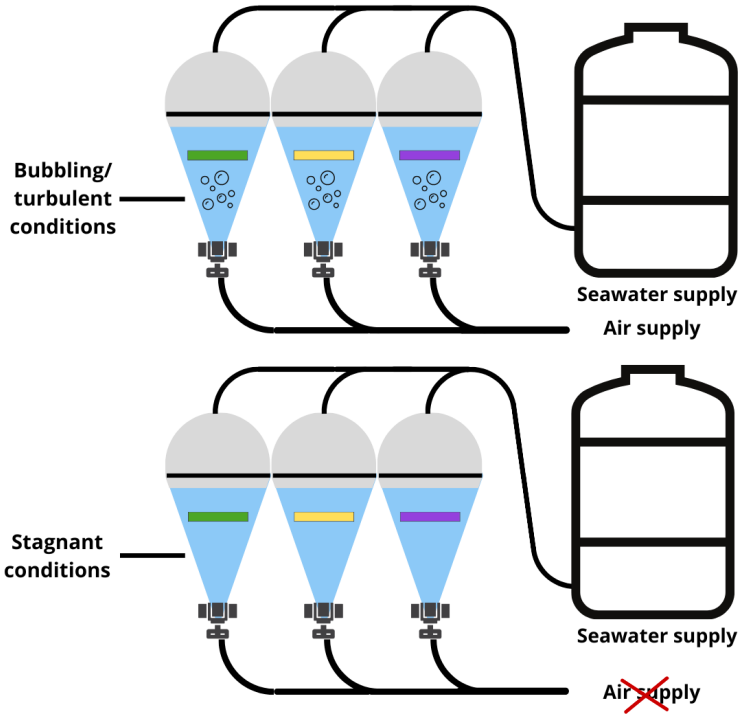

Figure 1: Sketch of the experimental setup and different treatments, that are olivine (green), sand (yellow), and olivine/sand (purple), each treatment in stagnant and under turbulent conditions. Each treatment was conducted in triplicates.

2.1.1.Sampling strategy and immediate fluid alkalinity and pH analyses

Fluids from the reactors were sampled twice on the first day (T+1h and T+6h), then daily for the first 7 days followed by sampling on day 9, 13 21. Additionally, three reference samples of the incoming seawater were taken on each sampling day and immediately analyzed for pH, temperature and salinity (WTW Multi 3630 IDS). Two separate samples were taken sequentially from each reactor by filling the sample bottles through the reactor outlet. A rinsed 60 ml low-density (LDPE) bottle was filled, and immediately measured for pH, temperature and salinity (WTW Multi 3630 IDS), followed by TA measurement via open-cell titration using an 888 Titrando (Metrohm) after filtration of the sample through a 0.7 um Whatman filter. The titrator electrode was calibrated using Tris buffer solution (T45 bottled in Dickson Lab) and titrator accuracy verified using Certified Reference Material (Dickson Lab, Batch 219). The second sample was taken in an acid-cleaned high-density (HDPE) bottles, filtered through a 0.2 µm filter (Cytiva) and acidified with 250 µL of ultrapure nitric acid (60%) for major and trace element analyses. The temperature of each reactor was measured daily using a temperature probe (Ebro TFX 410).

https://doi.org/10.5194/egusphere-2026-3096
Preprint. Discussion started: 10 June 2026

2.1.2. Major and trace element analyses

Major elemental analyses were conducted using an ICP-OES (Avio 500, Perkin Elemer; Utrecht University) with a conical spraychamber, a micro concentric Teflon nebulizer and a PrepFAST autosampler (SC-4 DX). Trace elements are measured using an ICP-MS (Nexion 2000p, Perkin Elemer) at Utrecht University with a cooled peltier conical spraychamber, a micro concentric Teflon nebulizer and a PrepFAST autosampler (SC-4 DX). For both instruments, all data are calculated with Indium as an internal standard. Every 12th measurements a drift standard (DRIFT) and quality check (QC) standard is measured. The LOD (limit of detection = 3 * SD from a blank signal) and LOQ (limit of quantification = 3 * LOD) are determined by measuring the blank for 10 times after the calibration is made.

2.2. Solid analyses

2.2.1. XRD

The mineralogical composition of the raw materials and of the reacted samples was determined via Rietveld refinement of X-ray diffraction (XRD) patterns recorded on a PANalytical X'Pert PRO diffractometer operated at 40 kV and 40 mA (Co-Kα) at Graz University. The instrument was equipped with a high-speed Scientific X'Celerator detector, 0.5° antiscattering and divergence slits, an automated sample changer magazine and a spinning stage. All samples were homogenized and finely ground using agate mortar and pestle prior to the analyses. The powders were prepared in standard XRD sample holders using the top-loading technique and a razor blade to avoid preferred particle orientation. The XRD measurements were done in the 2-Theta range between 4 and 85° using a step size of 0.08° 2-Theta and a step size of 40 s. The PANalytical X'Pert HighScore Plus software package and the ICSD database were used for mineral identification and quantification. The refined parameters included atomic coordinates, unit-cell dimensions, profile parameters, shape factors and preferred orientation, etc. The agreement parameters r_{wp} and GOF were always below 5 and 3, respectively. The analytical error is less than 2-3 wt.% for each mineral phase (Baldermann et al., 2013; Mendes et al., 2025).

2.2.2. XRF

The major and minor elemental composition of the materials, prepared as standard fused glass tablets, were analyzed by energy-dispersive X-ray fluorescence using a PANalytical Epsilon 4 X-ray spectrometer at Graz University. About 0.8 g of finely ground sample was heated to 1050 °C to remove volatiles, such as CO_2 and H_2O, and then the loss on ignition (LOI) was determined by gravimetric analysis. The residual was fused at 1200 °C in a LeNeo fusion instrument using 4 g of $LiBO_2$ as the fluent agent. The tablets were run together with a range of USGS standards and the analytical error determined to be better than ±0.5 wt.% for the major elements (Richoz et al., 2017). The detection limits of the minor and trace elements are ~0.1 wt% and ~50 ppm, respectively.

2.2.3. SEM

In order to check for physical grinding effects, one exemplary solid sample at the end of the experiments from the turbulent and stagnant olivine treatments was prepared for analysis using a Zeiss EVO Scanning Electron Microscope (SEM) at Utrecht University Electron Microscopy Facility, using an accelerating potential of 20 kV and a beam current of 500 pA at a working distance around 10 mm. Samples were mounted on aluminum stubs and coated with carbon prior to SEM analysis. The main

https://doi.org/10.5194/egusphere-2026-3096
Preprint. Discussion started: 10 June 2026

focus was to examine the effect of grain collision on grain morphology, presence of surface coatings and surface textures.

2.3 Carbonate system and thermodynamic equilibrium calculations

Carbonate chemistry was calculated based on measured TA, pH, T and salinity using the CO2SYS script for Excel (Pierrot et al., 2011). As input constants, we used the carbonic acid dissociation constants K_1 and K_2 from Lueker et al. (2000), bisulfate dissociation constant from Dickson (1990), the Boron-chlorinity ratio of Lee et al. (2010), and aragonite solubility constant by Mucci (1983). All pH values measured on the NBS scale were converted to the total scale using the pHnbs2total function in Matlab (V.2024b).

Thermodynamic equilibrium of primary and secondary silicates was calculated with PHREEQC using the Pitzer database (Parkhurst and Appelo, 2013).

2.4 Alkalinity correction measures

The amount of TA increase per treatment (ΔTA_{sw_cor}) was calculated with respect to the seawater reference by subtracting the average TA from the incoming seawater (sw) reference from the measured, average, TA in the individual treatments (pure olivine, pure sand and olivine/sand) for each sampling point:

$$\Delta TA_{sw\_cor} = TA_{treatment} - TA_{SW} \quad \text{Equ. 2}$$

The related uncertainty is calculated by error propagation of the standard deviation of the three replicates of the input values.

In order to evaluate the effect of sand grinding on olivine dissolution, several correction measures have to be made, which concern the amount of olivine used (11 g in pure olivine treatments and 2.2 g in olivine/sand treatments) and the effect of TA release from carbonate dissolution present in sand-amended treatments. Therefore, we subtract the sand ΔTA_{sw_cor} from the olivine/sand ΔTA_{sw_cor}, which represents the TA release solely stemming from olivine ($\Delta TA_{sw,sand\_cor}$):

$$\text{olivine}\Delta TA_{\text{sw,sand\_cor}} = \text{olivine/sand}\Delta TA_{\text{sw\_cor}} - \text{sand}\Delta TA_{\text{sw\_cor}} \quad \text{Equ. 3}$$

In a next step, the $\Delta TA_{sw,\ sand\_cor}$ from olivine was normalized to the amount of olivine used, correcting for the different amounts of the olivine starting in the pure olivine and olivine-sand treatment material (denoted as ol_cor $\Delta TA_{sw,\ sand\_cor}$).

In a following step, the alkalinity flux is calculated following:

$$F_x = \left(\frac{dC_x}{dt} + k_w * C_{out} - k_w * C_{in}\right) * V \quad \text{Equ. 4}$$

With F_x as the flux of any component (mol d^{-1}), $\frac{dC_x}{dt}$ is the property/concentration change of the respective component over a specific time (mol L^{-1} d^{-1}), k_w defines the water exchange rate (d^{-1}) calculated by dividing the flow rate by the reactor volume, C_{out} is the outflow concentration and C_{in} refers to the inflow concentration of the respective element (in mol kg^{-1} for TA and mol L^{-1} for element fluxes). V is the volume of the reactor (L). The derived flux (F_x) values were subsequently corrected

https://doi.org/10.5194/egusphere-2026-3096
Preprint. Discussion started: 10 June 2026

for the amount of olivine used (mol mol^{-1} olivine d^{-1}) and in the case of TA, the olivine/sand treatment for the sand contribution ($olivine/sandF_x - sandF_x$).

3. Results

3.1. Fluid geochemistry

The geochemical fluid data are presented as the average of the three replicates, and the error bar indicates one standard deviation (SD) between these replicates. Note that especially in the beginning of the experiment (first 48 hours) the SD is relatively high, showing the variance between the individual reactors. In the case of seawater (Equ. 2) or seawater, sand and olivine corrected data (Equ. 3), the propagated error is shown as uncertainty.

A strong rain event starting 24 hours to just before the last samples were taken (t = 480 hours) impacted the inflowing seawater composition, most visible in a drop in pH from 8.24 to 8.09 but also visible in decreasing TA values (Fig. 2). Therefore, we decided not to consider the data stemming from the last sampling points and focus the discussion on the experimental interval under similar ambient conditions.

3.1.1. Carbonate chemistry

Alkalinity: seawater corrected

Over the experimental period, TA varies above and below the incoming seawater reference TA (Fig. 2, supplementary Table S1). Especially within the first 48 hours, turbulent treatments from the olivine and olivine/sand experimental treatments yield highest TA increases with ΔTA_{sw_cor} of 102 µmol kg^{-1} and 78 µmol kg^{-1}, respectively (Equ. 2; Fig. 2, supplementary Table S1). After 48 hours (T+48h), TA decreases in both treatments and stabilizes to an apparent steady state. All remaining stagnant treatments as well as the turbulent sand treatments are within error equal to the seawater reference. Turbulent olivine, sand, and olivine/sand treatments yield similar apparent steady-state values of 23±11 µmol kg^{-1}, 18±8 µmol kg^{-1}, 25±9 µmol kg^{-1} (average of the last six samples, excluding the T+480h sample), respectively. All remaining stagnant treatments stay within error close to the seawater reference with apparent steady-state values of -2±7 µmol kg^{-1} for the olivine treatment, 5±5 µmol kg^{-1} for the sand treatment and -0.4±7 µmol kg^{-1} for the olivine/sand treatment (Fig. 2, supplementary Table S1).

https://doi.org/10.5194/egusphere-2026-3096
Preprint. Discussion started: 10 June 2026

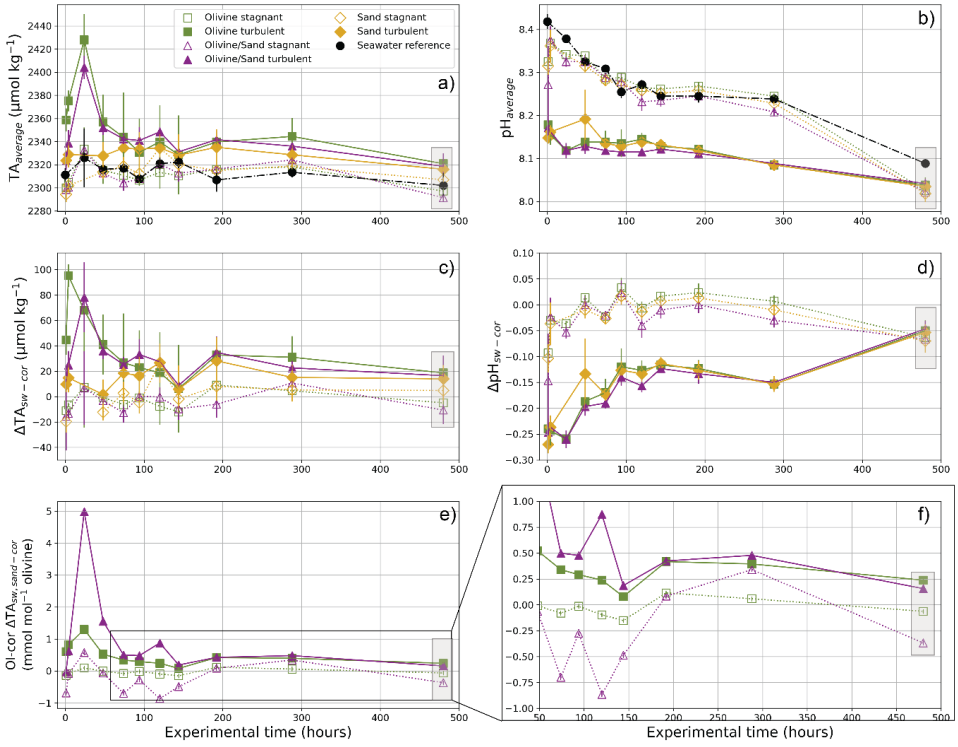

Figure 2: Measured (a) alkalinity (TA) and (b) pH data for the stagnant (empty symbols, dashed lines) and turbulent (full symbols, solid lines) beach simulation experiments as well as the seawater reference. Seawater *corrected* data is shown for (c) alkalinity and (d) pH. (e) Alkalinity release normalized for the amount of olivine in the different olivine treatments and corrected to TA seawater and sand and (f) zoom for t > 50hours. For (a) and (b) data points are the average of the three replicates and error indicates 1 standard deviation (1 SD) of the replicates. For subplots (c) to (f), the data points are the average of the three replicates and the error bar is the propagated error from the treatments and seawater reference. In (e) and (f), error bars within symbol size; note the unit change. Grey boxes highlight the ignored data that were affected by an extreme rain event just prior the sampling time, impacting ambient conditions (section 4.1). A general trend of higher alkalinity release and lower pH is observed for the turbulent treatments compared to the stagnant treatments.

Alkalinity: amount olivine normalized

With respect to the amount of olivine used in the different olivine treatments, the TA release was highest in the turbulent olivine/sand treatments with 5.0 mmol mol^{-1} olivine (note that the sand TA contribution is subtracted (Equ. 3)) (Fig. 2). The pure olivine treatment yields an ol_cor$\Delta TA_{sw,\ sand_cor}$ of 1.3 mmol mol^{-1} olivine. Apparent steady state ol_cor$\Delta TA_{sw,\ sand_cor}$ values yield 0.3±0.1 mmol mol^{-1} olivine for the pure olivine treatment and yield 0.5±0.4 mmol mol^{-1} olivine for the olivine/sand treatment. All stagnant treatments remain within error to the seawater reference.

https://doi.org/10.5194/egusphere-2026-3096
Preprint. Discussion started: 10 June 2026

Alkalinity: fluxes

The highest TA fluxes were observed in the turbulent olivine/sand treatment with 11 mmol mol^{-1} olivine day^{-1} (after T+24h), followed by the stagnant olivine/sand treatment with 5.0 mmol mol^{-1} olivine day^{-1} (after T+4h) and the turbulent olivine treatment with 3.8 mmol mol^{-1} olivine day^{-1} (Fig. 3, Table 1, supplementary Table S2). After this initial peak with TA fluxes decline to an average (last 6 sampling times) of 1.1±0.6 mmol mol^{-1} olivine day^{-1} for the turbulent olivine/sand treatment, -0.9±1.3 mmol mol^{-1} olivine day^{-1} for the stagnant olivine/sand treatment and 0.7±0.3 mmol mol^{-1} olivine day^{-1} for the turbulent olivine treatment.

The stagnant olivine treatment shows the lowest overall TA flux with an average value of 0.02±0.3 mmol mol^{-1} olivine day^{-1}, over the entire experiment.

The turbulent and stagnant sand treatments overlap within error with average fluxes of 0.04±0.02 mmol mol^{-1} olivine day^{-1} and 0.01±0.01 mmol mol^{-1} olivine day^{-1}, respectively.

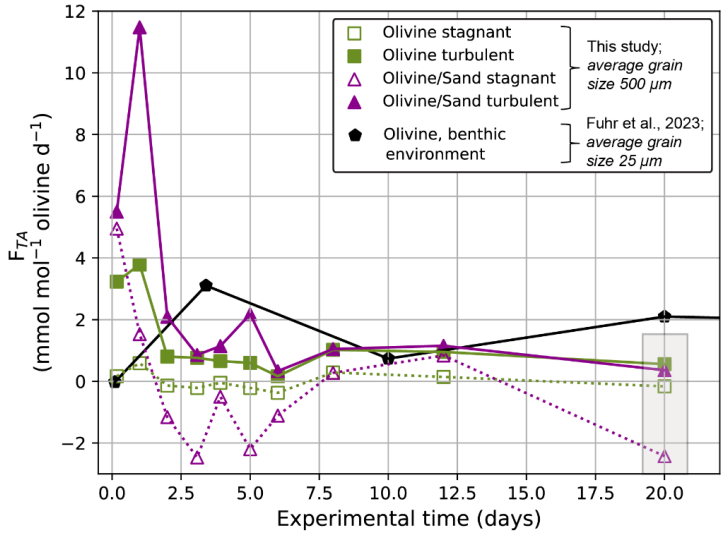

Figure 3: Alkalinity (TA) fluxes for the stagnant and turbulent olivine and olivine/sand treatments. Grey box indicates an extreme rain event during the sampling time, impacting ambient conditions (section 4.1). For comparison, the TA fluxes from core incubation experiments are shown, in which olivine dissolution was enhanced by microbial activity, simulating the low-energy shelf environment (Fuhr et al., 2023).

https://doi.org/10.5194/egusphere-2026-3096
Preprint. Discussion started: 10 June 2026

Table 1: Fluxes per day for the stagnant and turbulent beach simulation experiments. Note the different units for Ni and Cr compared to TA, and that olivine treatments are normalized to the amount olivine used, while sand fluxes are solely reported in nmol per day. Error is the standard deviation (1SD) of the last 2 sampling intervals excluding the last one at T+480h (see section 3.1).

Sample	Highest TA flux mmol mol^{-1} olivine day^{-1}	Average TA flux last 2 s.i.[a] mmol mol^{-1} olivine day^{-1}	1SD	Highest Ni flux nmol mol^{-1} olivine day^{-1}	Average Ni flux last 2 s.i.[a] nmol mol^{-1} olivine day^{-1}	1SD	Highest Cr flux nmol mol^{-1} olivine day^{-1}	Average Cr flux last 2 s.i.[a] nmol mol^{-1} olivine day^{-1}	1SD
Olivine stagnant	0.59	0.21	0.10	1175	697	291	225	-78	76
Olivine turbulent	3.79	0.99	0.05	12486	2022	153	4559	1061	60
Olivine/sand stagnant	4.95	0.56	0.40	104	87	7	288	-77	19
Olivine/sand turbulent	11.5	1.10	0.07	1212	86	36	1614	115	118
	mmol day^{-1}	mmol day^{-1}		nmol day^{-1}	mmol day^{-1}		nmol day^{-1}	mmol day^{-1}	
Sand stagnant	0.04	0.02	0.00	54	28	6	10	-4.9	0.2
Sand turbulent	0.07	0.05	0.02	593	22	1	186	-5.3	3.3

[a]Sampling intervals (s.i.)

pH variation and seawater corrected

The seawater total pH decreased over the course of the experiment from 8.42 to 8.24 at T+288h (Fig. 2, supplementary Table S1). All stagnant treatments show a similar trend, being about 0.1 pH units lower (ΔpH_{sw_cor}, normalized in the same way as for TA) in the first 4 hours of the experiment, and then remain within error similar to incoming seawater pH. All turbulent treatments decreased from pH of ~8.17 at T+1 (ΔpH_{sw_cor} of -0.25 after 1 hour) to a pH of 8.09 (ΔpH_{sw_cor} of -0.15) after T+288h and, therefore, remained below incoming seawater pH throughout the experiment. Interestingly, at the end of the experiment during the rain event, all stagnant and turbulent treatments attained a similar pH of 8.02, that is 0.07 pH units (ΔpH_{sw_cor}) lower than incoming seawater pH with 8.09.

DIC, pCO2 and Ω_A

Calculated DIC values follow a similar trend compared to pH, with all stagnant treatments following the seawater concentration trend, which ranged between 1908 µmol kg^{-1} and 2092 µmol kg^{-1} (Fig. 4, supplementary Table S1). Turbulent treatments were higher in DIC compared to the incoming seawater reference and ranged between 2016 µmol kg^{-1} and 2152 µmol kg^{-1}, with olivine and olivine/sand treatments showing a peak at T+24h while the sand treatment decreased. After about T+100 h, all turbulent treatments showed a continuous increase in DIC, which was also reflected in the pH signal.

A similar pattern is also visible in the pCO_2 data, showing lower values for the seawater and stagnant treatments (between 135 µatm and 422 µatm) compared to the turbulent treatments (between 266

https://doi.org/10.5194/egusphere-2026-3096
Preprint. Discussion started: 10 June 2026

µatm and 404 µatm). All treatments and the seawater reference increase in pCO_2 throughout the experiment.

All treatments and the seawater reference were oversaturated with respect to aragonite ($\Omega_{Ar} > 1$) (Fig. 4, supplementary Table S1). At T+4h, Ω_{Ar} showed the largest variation between 3.0 (turbulent sand) and 4.4 (stagnant olivine) for all treatments, which was lower than the incoming seawater reference, which decreased in Ω_{Ar} from 4.7 (T+1h) to 3.6 (T+288h). In the course of the experiment, all treatments showed decreasing Ω_{Ar}, with stagnant treatments reaching higher Ω_{Ar} (between 4.4 and 3.4) than the turbulent treatments (between 3.2 and 2.7)— except the last sampling point— where stagnant treatments decreased to values slightly lower than turbulent treatments.

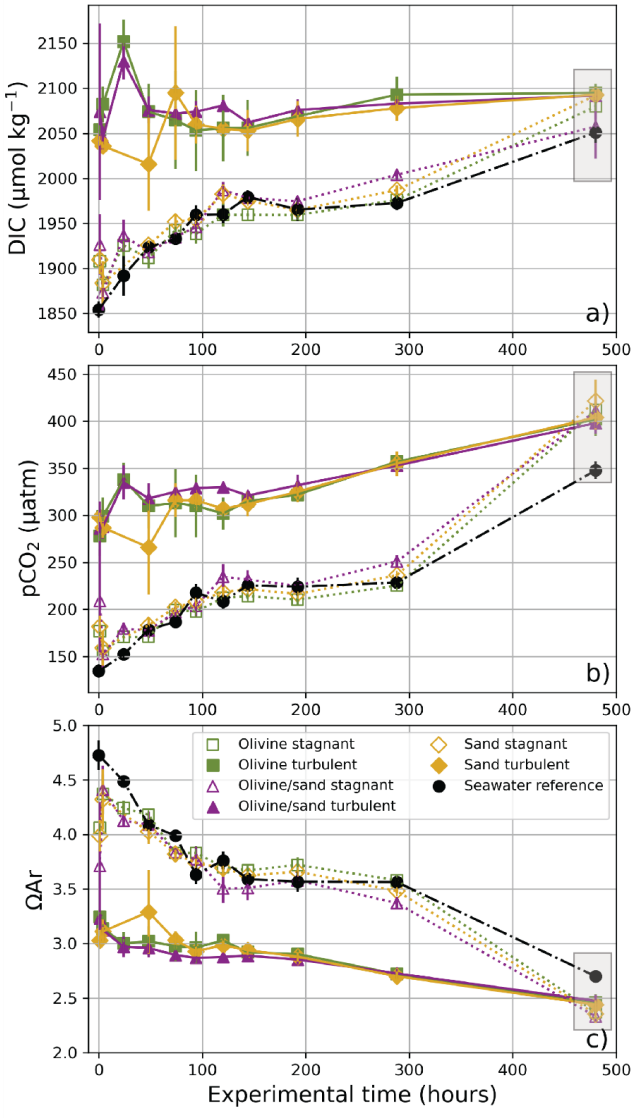

https://doi.org/10.5194/egusphere-2026-3096
Preprint. Discussion started: 10 June 2026

Figure 4: Calculated carbonate system parameters (a) DIC, (b) pCO_2 and (c) Ω_{Ar} following TA and pH input values using the system CO2SYS for the stagnant (empty symbols, dashed lines) and turbulent (full symbols, solid lines) beach simulation experiments as well as the seawater reference. Data points are the average of the three replicates and error indicates 1 SD of the replicates. Grey box indicates an extreme rain event during the sampling time, impacting ambient conditions (section 4.1).

3.1.2. Major and trace element concentrations

The major seawater cations Ca, Na, and K did not show any significant variation between all treatments and the incoming seawater reference (supplementary Fig. S1 and Table S3). For the sand-bearing treatments, Mg concentrations increased for all turbulent and stagnant treatments relative to the incoming seawater reference over the experimental period (supplementary Fig. S1). Silicon (Si) and total dissolved iron (Fe) concentrations were highest in the first 100 hours of the experiment with maximum values from the turbulent olivine treatments at 178 µmol L^{-1} and 29.5 nmol L^{-1}, respectively (Fig. 5a,b). In the case of Si, most treatments were below detection limit after T+100h. Lithium (Li) and strontium (Sr) showed distinct patterns for the sand-bearing treatments, while the olivine pure treatments stayed within error of the incoming seawater reference, with the exception of an increase in Li in the first 4 hours (Fig. 5c,d). For the turbulent and stagnant sand-bearing treatments, Li increased within the first 120 hours to a maximum value of 32 µmol L^{-1}, and then decreased to 28 µmol L^{-1} (turbulent sand treatments). In all sand-bearing treatments, Sr increased continuously over the course of the experiment with highest concentrations reaching 112 µmol L^{-1} after T+288h for the olivine/sand treatment. Similarly to Li, Sr concentrations in olivine pure treatments stayed within error to the incoming seawater reference (Fig. 5c,d; supplementary Table S3).

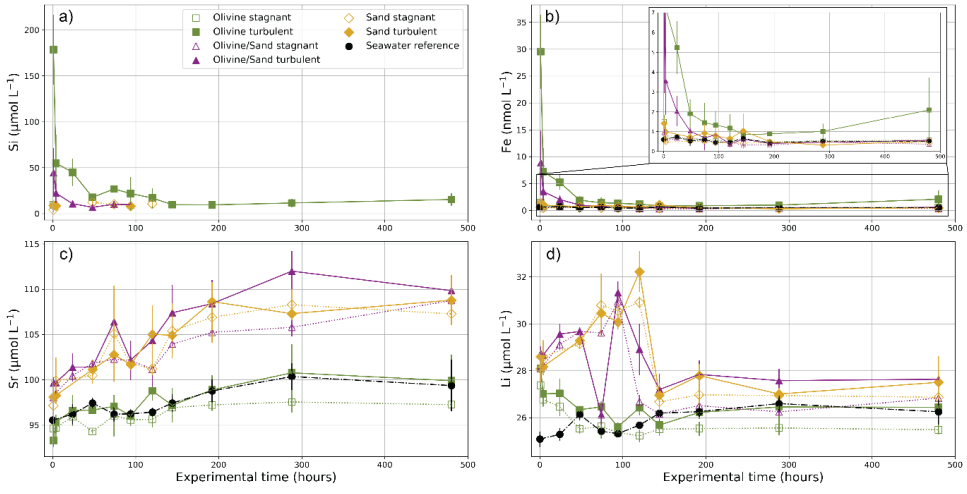

Figure 5: Major and trace element data for the different treatments of the beach simulation experiments, with (a) magnesium (Mg), (b) silicon (Si), (c) iron (Fe) and (d) and strontium (Sr). Data points are the average of the three replicates and error indicates 1 SD of the replicates. Note the high Si and Fe concentrations of all olivine-bearing treatments in the beginning of the experiment and the increase Sr in all sand-bearing treatments.

https://doi.org/10.5194/egusphere-2026-3096
Preprint. Discussion started: 10 June 2026

Turbulent olivine treatments showed highest concentrations in Ni (1632 nmol L^{-1}) and Cr (896 nmol L^{-1}), followed by the turbulent olivine/sand treatment with 359 nmol L^{-1} for Ni and 171 nmol L^{-1} for Cr. Subsequently, concentrations decreased over the course of the experiment for the turbulent olivine treatments to apparent steady-state values of 66±4 nmol L^{-1} and 47±7 nmol L^{-1}, respectively (supplementary Table S3, Fig. 6). This was still 50 nmol L^{-1} for Ni and 31 nmol L^{-1} for Cr greater than incoming seawater. Ni and Cr concentrations for the turbulent olivine/sand treatment decreased to average values of 18±1 nmol L^{-1} and 19±3 nmol L^{-1}, respectively, within error similar to the seawater reference (Ni: 15±3 nmol L^{-1}; Cr: 16±2 nmol L^{-1}). All stagnant treatments and the turbulent sand treatments stayed within error similar to the seawater reference.

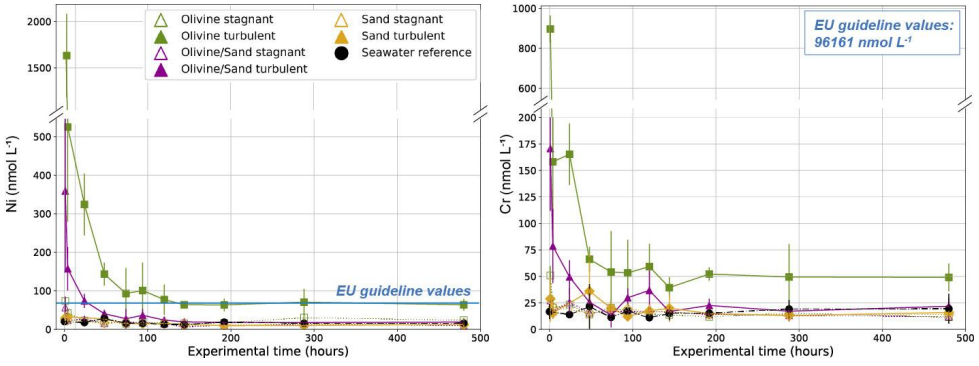

Figure 6: Trace metal data for the different treatments of the beach simulation experiments, with (a) nickel (Ni) and (b) chromium (Cr). Data points are the average of the three replicates and error indicates 1 SD of the replicates.

3.1.3.Major and trace element fluxes

The highest Si fluxes were reached for the turbulent olivine treatment with Si at 1.4 mmol mol^{-1} olivine day^{-1}, Fe (142 nmol mol^{-1} olivine day^{-1}), Ni (12.5 µmol mol^{-1} olivine day^{-1}) and Cr (4.6 µmol mol^{-1} olivine day^{-1}) (Table 1, supplementary Figure S2 and Table S3). These fluxes quickly declined over the course of the experiment where minimum values were recorded: Si (0.29 mmol mol^{-1} olivine day^{-1}), Fe (10.2 nmol mol^{-1} olivine day^{-1}), Ni (1.92 µmol mol^{-1} olivine day^{-1}) and Cr (0.71 µmol mol^{-1} olivine day^{-1}). Fluxes of the turbulent olivine/sand treatment were lower compared to the pure olivine treatment with the highest values reaching 0.61 mmol mol^{-1} olivine day^{-1} for Si, 74.7 nmol mol^{-1} olivine day^{-1} for Fe, 1.21 µmol mol^{-1} olivine day^{-1} for Ni and 1.61 µmol mol^{-1} olivine day^{-1} for Cr. Similarly to the turbulent olive treatment, these fluxes subsequently declined and merged to match those of the stagnant olivine and olivine/sand treatments: 0.30 mmol mol^{-1} olivine day^{-1} for Si, -5.25 nmol mol^{-1} olivine day^{-1} for Fe, -0.003 µmol mol^{-1} olivine day^{-1} for Ni and 0.02 µmol mol^{-1} olivine day^{-1} for Cr (Table 1, supplementary Figure S2 and Table S3).

In contrast, Sr and Li maximum fluxes were recorded in the turbulent and stagnant olivine/sand treatments. For Sr, fluxes increased throughout the experiment with the highest values recorded for the turbulent olivine/sand treatment, ranging from 70 to 445 µmol mol^{-1} olivine day^{-1}. Whereas the Li fluxes initially increased in the beginning of the experiment at T+4h from 87 to 168 µmol mol^{-1} olivine day^{-1} (excluding the extreme decrease of one sampling point to 8 µmol mol^{-1} olivine day^{-1} at T+74 h). Fluxes then declined after T+120h to a minimum of 54 µmol mol^{-1} olivine day^{-1}. Fluxes for the turbulent

https://doi.org/10.5194/egusphere-2026-3096
Preprint. Discussion started: 10 June 2026

and stagnant olivine treatments were generally lower than the sand-bearing treatments, and ranged from -81 (stagnant) to 103 (turbulent) µmol mol^{-1} olivine day^{-1} for Sr, and varied between -18 (stagnant) and 37 (turbulent) µmol mol^{-1} olivine day^{-1} for Li (supplementary Table S3).

For the stagnant and turbulent sand treatments, Fe fluxes remained mostly around zero, except for peaks observed in the turbulent treatments reaching a flux of 11 µmol day^{-1}. Si fluxes are only detectable in the beginning of the experiments, and ranged from -1.01 (stagnant) to 112 (turbulent) µmol day^{-1} (supplementary Table S3). Sr concentrations increased from 2.2 to 27.3 µmol day^{-1}, while Li concentrations varied between 2.01 and 15.4 µmol day^{-1}. Ni fluxes varied between 22 (stagnant) and 593 (turbulent) nmol day^{-1} and between -5.2 and 186 (turbulent) nmol day^{-1} for Cr (supplementary Table S3).

3.2. Solid composition and geochemistry

3.2.1. Mineralogy

The initial (i.e., before the experiment) olivine composition was 93 wt.% olivine and 3.9 wt.% pyroxene, with traces of kaolinite (1.0 wt.%), antigorite (0.8 wt.%), chlorite (0.6 wt.%), muscovite (0.5 wt.%) and talc (0.4 wt.%) (supplementary Figure S3 and Table S4). The sand starting material was composed of 49 wt.% quartz, 19 wt.% plagioclase and 11 wt.% microcline, with minor components of calcite (7.6 wt.%), halite (4.8 wt.%), aragonite (4.4 wt.%), high Mg-calcite (1.5 wt.%) and muscovite (1.5 wt.%).

The stagnant and turbulent olivine and sand treatments were within error similar to the initial compositions, showing no significant compositional changes after the experiment (supplementary Figure S3 and Table S4). The stagnant and turbulent olivine/sand treatments (mixture of 2.2 g and 8.8 g, respectively) showed no mineralogical differences and were composed of, on average, 38 wt.% quartz, 23 wt.% olivine, 2.4 wt.% pyroxene, 14 wt.% plagioclase, 9 wt.% microcline, with minor components of calcite (5.3 wt.%), aragonite (3.3 wt.%), halite (1.7 wt.%), high Mg-calcite (1.5 wt.%) and muscovite (1.5 wt.%).

3.2.2. Geochemistry

The olivine was composed of 41.25 wt.% SiO_2, 49.38 wt.% MgO and 7.75 wt.% Fe_2O_3. All other major elements were <1 wt.%. Olivine was enriched in the trace metals Cr (1912 ppm), Ni (3193 ppm) and Zn (51 ppm). The initial sand composition was 61.49 wt.% SiO_2, 10.55 wt.% CaO, 9.64 wt.% Al_2O_3, 3.70 wt.% K_2O and 2.06 wt.% Na_2O. All other major elements were <1 wt.%. Trace elements in the sand yielded 730 ppm Sr, 364 ppm Ba, 143 ppm Rb and 59 ppm Zr(supplementary Figure S4 and Table S5).

After the experiment, the geochemistry of the solids in the olivine and sand treatments (turbulent and stagnant) were within error similar to the initial composition (supplementary Figure S4; supplementary Table S4). The stagnant and turbulent olivine/sand mixtures were within error similar in their composition with respect to the major elements. For the trace metals, Ni in the turbulent olivine/sand treatment showed higher concentrations (835 ppm) compared to the stagnant treatment (675 ppm) (supplementary Figure S5; supplementary Table S5). In the turbulent treatment, concentrations were 469 ppm for Sr, 242 ppm for Cr, 116 ppm for Rb and 238 ppm for Ba. In the stagnant olivine/sand treatment, trace element concentrations were 534 ppm for Sr, 321 ppm for Cr, 233 ppm for Ba and 114 ppm for Rb.

https://doi.org/10.5194/egusphere-2026-3096
Preprint. Discussion started: 10 June 2026

Correction of the trace metals to the initial composition showed a depletion of -570 ppm for Cr and an enrichment of +42 ppm for Ni in the turbulent olivine treatment (supplementary Figure S5). Whereas, for the sand treatment, the corrected sand treatments showed a depletion for Sr of -49 ppm and -74 ppm for the turbulent and stagnant experimental runs, respectively. The turbulent olivine/sand treatment showed enrichment in Ni of +196 ppm and depletions in of Cr (-140 ppm), Sr (-115 ppm) and Ba (-54 ppm). The stagnant olivine/sand treatment showed enrichment in Ni of +36 ppm and depletions of Cr (-62 ppm), Sr (-51 ppm) and Ba (-58 ppm) (supplementary Figure S6).

3.2.3. Mineral surface texture and element composition

The grain morphology differed significantly between the turbulent and stagnant olivine treatment. In the turbulent olivine treatment, the grains showed rounded edges, abrasion pits and striation-like features compared to the stagnant olivine treatment (Fig. 7). The abrasion pits appear as shallow, irregular depressions of varying size, commonly concentrated along the grain edges and high-relief areas, suggesting repeated mechanical impact or directional contact. The olivine grains from the stagnant treatment showed a rough surface texture and sharp edges (Fig. 7a,b). Despite halite, which likely originated from drying of the samples, no surface precipitates were observable on the olivine grains.

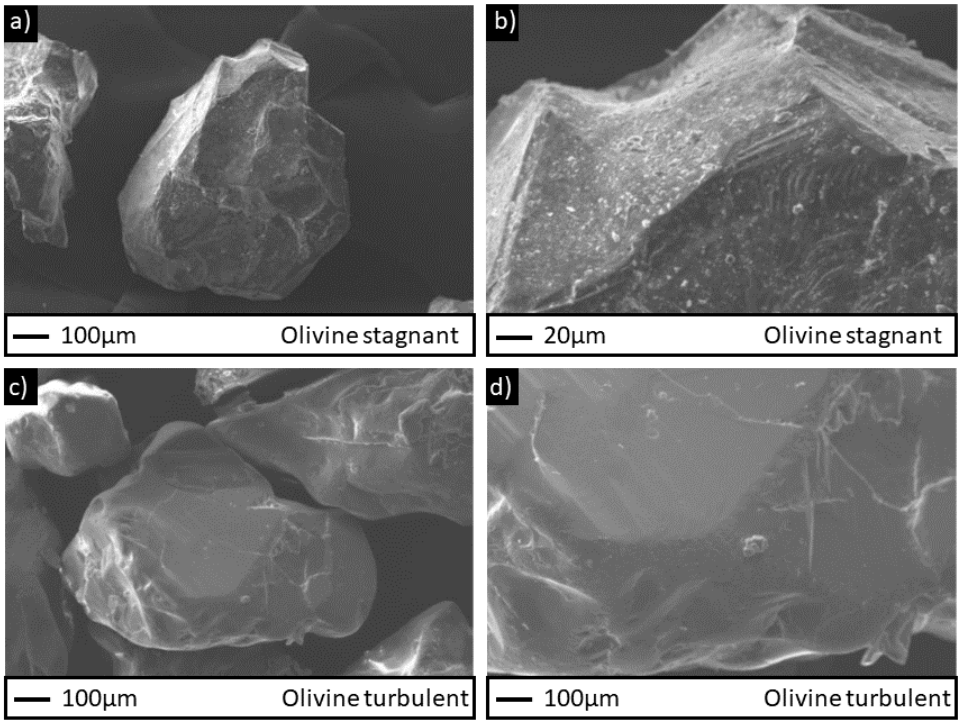

Figure 7: Secondary Electron Microscopy images of olivine grains from the stagnant (a,b) and turbulent (c,d) experimental treatment. In the turbulent olivine treatment, grain edges are more rounded compared to olivine grains from the stagnant treatment, indicating the effect of abrasion due to grain collision.

https://doi.org/10.5194/egusphere-2026-3096
Preprint. Discussion started: 10 June 2026

3.2.4. Saturation indices for secondary phyllosilicates

Amorphous silica ($SiO_{2(a)}$) was undersaturated throughout the whole experiment for the turbulent olivine treatment (saturation indices (SI) from -1.0 (T+1h) to -2.1 (T+280h)), between -2.6 (T+1h) and -2.3 (T+94h) for turbulent and stagnant sand and until T+94h for the olivine/sand treatment (SI from -1.6 (T+1h) to -2.2 (T+94h); supplementary Figure S7). Note that for the stagnant and turbulent (T>94h) olivine/sand, sand and the stagnant olivine treatments (except T+1h with -2.2), no saturation indices could be calculated because of the low (below detection limit) Si concentrations (supplementary Table S3). Consequently, Si-phases, in general, were undersaturated for these experimental treatments. Amorphous silica ($SiO_{2(a)}$) was also undersaturated throughout the experiment for all treatments, ranging in SI from -1 (T+1h, turbulent olivine) to -2.6 (T+94h, stagnant sand). Sepiolite and $Fe(OH)_3$ were only oversaturated in the first 4 hours of the turbulent olivine treatment; SI up to 1.6 and 0.17, respectively.

Chrysotile was oversaturated for the turbulent olivine treatment throughout the whole experiment (SI between 0.04 and 3.0) and, in case where Si concentrations could be measured, for the turbulent olivine/sand (SI between 0.1 and 1.7; except T+48h with -0.1) and stagnant and turbulent sand (SI between 0.5 and 1.0 and 0.3 and 0.02, respectively) treatments (supplementary Figure S7).

4. Discussion

In coastal environments, the high-energy surf zone is considered a potential OAE deployment site, in which the effect of grain collision is hypothesized to enhance mineral dissolution and, thus, increase TA. Below, we will discuss the effectiveness of this approach using the results of the flow-through experiments that were designed to mimic the surf zone, fostering efficient grain collision and providing high dilution factors with ambient seawater. However, before the efficiency of this OAE approach is discussed, some experimental artefacts are considered that are impacting the carbonate system.

4.1. Carbonate system and experimental challenges

The experimental set up of the turbulent reactors caused several artefacts that potentially impacted the geochemical conditions in the reactors. The constant bubbling with ambient air in the turbulent reactors injected atmospheric CO_2 with the inflowing seawater while facilitating CO_2 exchange between the water line and headspace in the reactor. This shifted the pCO_2 in the turbulent reactors to higher values (average last three data points 332±18 µatm) compared to the stagnant reactors (226±13 µatm) (Fig. 4b). The turbulent reactors were therefore affected by atmospheric CO_2 invasion— but like the natural conditions in a surf zone— while the stagnant reactors followed the trend of the inflowing seawater. The similarity of stagnant and incoming pCO_2 demonstrates that influx was more important than an exchange within the headspace and any potential slow dissolution occurring in the stagnant cones. That is, mixing of incoming seawater with the reactor fluid was a more primary driver of TA flux in the stagnant, passive, system.

Interestingly, the DIC values of the inflowing seawater and the stagnant treatments were lower than the long-term concentration values for the west coast off Brittany (ranging seasonally and locally between about 2050 and 2200 µmol kg^{-1} recorded during the years 2008 and 2020; Gac et al. (2021); Petton et al. (2024)). This might be caused by phytoplankton activity (photosynthesis) in the outside

https://doi.org/10.5194/egusphere-2026-3096
Preprint. Discussion started: 10 June 2026

pond where incoming seawater is pumped into the experimental laboratory at Ifremer. This effect was not visible in the turbulent treatments where the carbonate system was affected by the bubbling with CO_2 in the reactors. Over the course of the experiment, we saw an increase in DIC and pCO_2 that translated to a decrease in pH, which was likely caused by CO_2 invasion from the injected air stream (Fig. 4a,b; 8). Following the carbonate system processes and their stochiometric influences on TA and DIC, all stagnant treatments and the seawater reference followed the CO_2 invasion trendline with some treatments indicating carbonate dissolution (Fig. 8). The turbulent treatments cluster to the upper right with respect to the starting seawater composition, and even fall on the carbonate dissolution trend line. However, we exclude carbonate dissolution as a process affecting our experiments because (1) olivine-bearing treatments do not contain carbonates (supplementary Fig. S2 and Table S4), and (2) carbonate was oversaturated throughout the experiment, (i.e., no dissolution; Fig. 4c). We conclude that the olivine and olivine/sand treatments were impacted by a mixture of olivine dissolution (only adding TA) and CO_2 invasion (only adding DIC), while the sand pure treatments were impacted by CO_2 invasion and other dissolving mineral phases, likely feldspars (see following section 4.2).

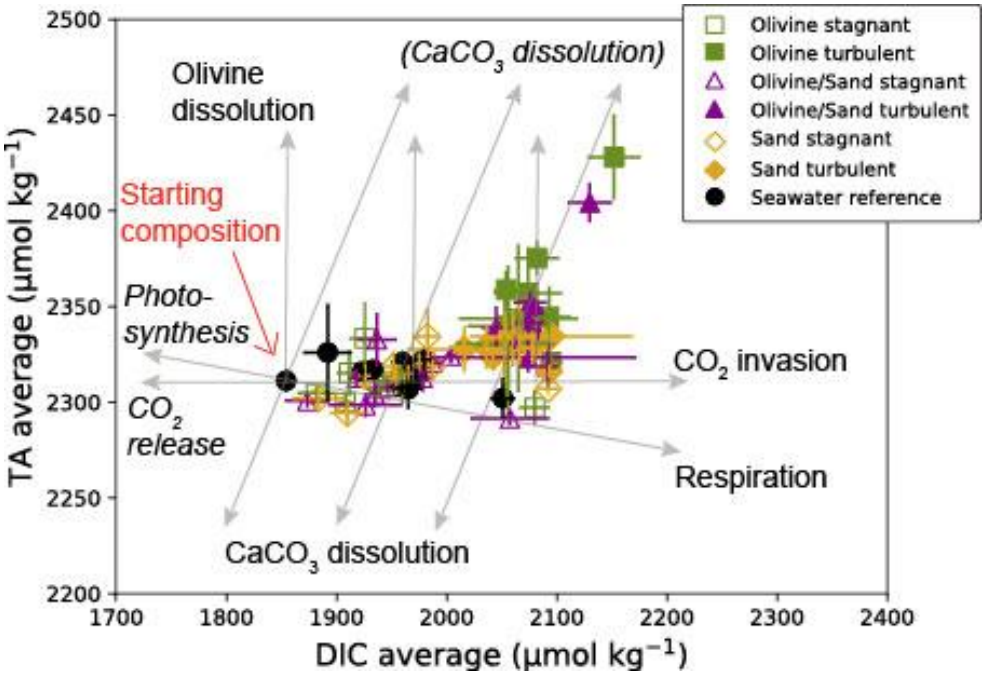

Figure 8: Alkalinity (TA) versus DIC and indicated carbonate-affecting processes modified after Zeebe and Wolf-Gladrow (2006). Experimental samples are mostly affected by CO_2 invasion as well as olivine dissolution with minor carbonate precipitation. Processes indicated in italic do not apply to our experimental results. Note that carbonate dissolution is unlikely to occur due to $\Omega > 1$ for all treatments.

https://doi.org/10.5194/egusphere-2026-3096
Preprint. Discussion started: 10 June 2026

4.2. Effectiveness of grain collision on mineral dissolution and alkalinity generation

The effect of grain collision, providing a natural grinding mechanism, is clearly visible in the results of our experiments. All turbulent experimental treatments show a higher TA and flux compared to the stagnant treatments (Fig. 2,3; Table 1). This indicates that turbulent conditions are enhancing alkalinity generation, and can be regarded as an efficient application for OAE beach deployments. The generated TA (corrected to background seawater and normalized to mass of olivine; ol_corΔTA $_{sw, sand\_cor}$; see section 2.4), was higher in all turbulent compared to stagnant treatments, approaching an average TA concentration for the olivine and olivine/sand treatment of 0.41±0.02 and 0.45±0.04 mmol mol^{-1} olivine, respectively (Fig. 2e,f; supplementary Table S1). This was excluding an initial TA peak of up to 5.0 mmol mol^{-1} olivine for the olivine/sand treatment. This initial TA peak, however, has also been seen in experiments by Flipkens et al., 2023), who used the same type of olivine, though with a smaller average grain size (between 84 and 250 µm). Therefore, it is likely that this initial TA peak is related to the dissolution of fine-grained olivine material, following the common assumption, that with a higher surface area the dissolution rates increase compared to larger sized particles with a smaller surface area.

Amongst all turbulent treatments, the olivine/sand treatment reached the highest TA flux at 11.5 mmol mol^{-1} olivine d^{-1}, while the olivine treatment yielded 3.8 mmol mol^{-1} olivine d^{-1} (T+24h; Table 1). This high TA increase in the olivine-bearing treatment is either caused by a larger fraction of small olivine particles (<250 µm), that make up 11.4 wt% of the total used olivine (section 2.1), or by fast mineral reaction rates in the beginning of the experiment when minerals are far-from-equilibrium when first brought in contact with seawater (Jeandel and Oelkers, 2015).

For the stagnant treatments, TA either remained mostly within error to the incoming seawater reference (olivine treatment) or even showed negative TA values and fluxes (olivine/sand treatment; Figure 2, 3). The drop in TA below seawater concentration could be indicative of calcium carbonate mineral precipitation, which would also align with the oversaturated conditions of the fluids, with respect to aragonite (between 3.4 and 4.4). Moras et al. (2022) found in lime dissolution experiments, that carbonate precipitation was only triggered at Ω_{Ar} larger than 7, which is higher than the saturation value observed in our experiments. However, under the stagnant conditions in our experiment, the olivine and sand mixture remained undisturbed at the bottom of the reactor, providing nucleation sites, and localised carbonate mineral saturation in the pore space could exceed that based on the measured TA in the outflowing solution, potentially triggering carbonate mineral precipitation.

Towards the end of the experiment, TA fluxes were a magnitude lower at 1.1±0.1 mmol mol^{-1} olivine d^{-1} for the turbulent olivine/sand treatment and 1.0±0.05 mmol mol^{-1} olivine d^{-1} for the turbulent olivine treatment (Fig. 3, Table 1). Both treatments overlapped in their TA fluxes within error; therefore, the effect of sand grinding diminished with time. This could be due to the grinding effect and the grain rounding where the sharp edges and loose particles become erased. Quartz, the main component of our sand (supplementary Table S4), has a slightly higher hardness (Mohs Scale (MS): 7) compared to olivine (MS: 6.5-7). This could generate the extra abrasion and, thus, trigger higher TA generation in the olivine/sand mixture treatments compared to the olivine pure treatments in the beginning of the experiment.

When comparing the observed TA fluxes of the high-energy beach deployment simulation to fluxes observed by Fuhr et al. (2023) in from flow-through experiments simulating the low-energy benthic environment, we see a ~3-times higher TA generation in the beach simulation (11.5 mmol mol^{-1} olivine d^{-1}). That is, in Fuhr et al. (2023) olivine dissolution was promoted by microbial activity in their low-energy simulation (average of Dun1 & Dun2: 3.6 mmol mol^{-1} olivine d^{-1}), whereas the high-energy

https://doi.org/10.5194/egusphere-2026-3096
Preprint. Discussion started: 10 June 2026

environment in our study displayed a magnified dissolution effect. Interestingly, both TA fluxes decreased to a similar value after 10 experimental days (~1 mmol mol^{-1} olivine d^{-1}), while the benthic low-energy experiments increased again to attain an apparent steady-state of ~2.2 mmol mol^{-1} olivine d^{-1}. However, it is important to note that the benthic low-energy experiments used a much smaller grain size (20-30 µm; Fuhr et al. (2023) compared to the high-energy beach experiments of this study (average of 500 µm). Therefore, the TA fluxes of the two experiments cannot be directly compared. Still, the results highlight the effectiveness of grain collision enhanced mineral dissolution, as similar steady-state TA fluxes are attained with a ~15-times larger grain size. This finding has important implications for the Life Cycle Assessment (LCA) of coastal enhanced weathering, as costs and energy can be saved with respect to mineral grinding before deployment (Foteinis et al., 2023). Further, it would be within reason to think that if smaller grain sizes were used in this study, our observed TA fluxes would be even greater due to the faster dissolution of grains with a lower specific surface area and additional grinding effect.

In addition to an effective grain abrasion process, we see an enhanced dissolution behaviour, due to the constant exchange with seawater caused by the flow-through experimental design compared to batch experimental setups (Flipkens et al., 2023; England and Bach, 2025). In the batch experiments of recent studies, in which the effect of grain collision on either pure olivine (Flipkens et al., 2023) or pure olivine and a mixture of olivine and sand (England and Bach, 2025), an increase in alkalinity was observed. In all of these set ups, however, the TA accumulation was lower compared to our flow-through experimental results (Fig. 9). In conclusion, our experiments confirm the effectiveness of grain collision on TA generation, and in addition to the previous batch studies, show the enhanced mineral dissolution by constant dilution with seawater.

https://doi.org/10.5194/egusphere-2026-3096
Preprint. Discussion started: 10 June 2026

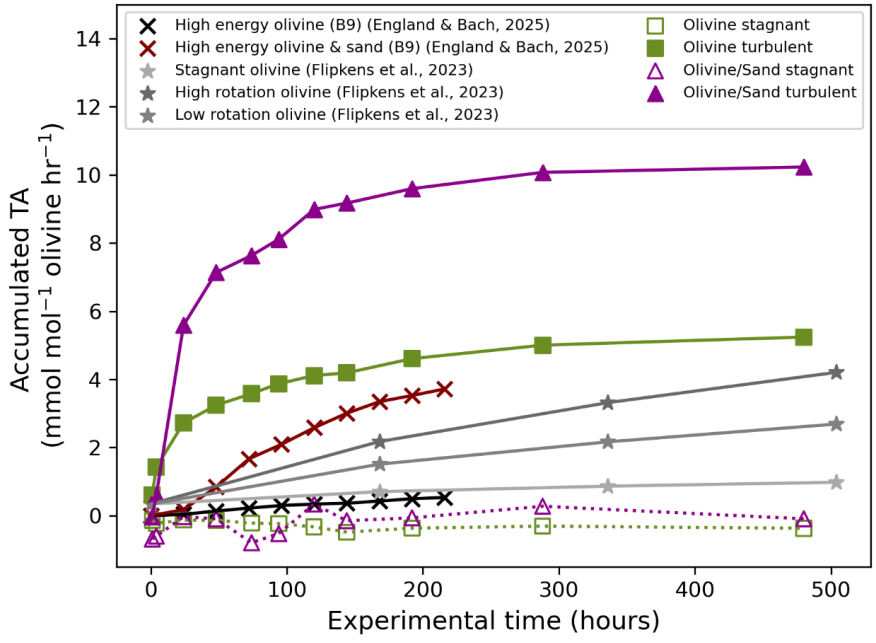

Figure 9: Accumulated TA increase over the course of the experiments. Turbulent TA release of olivine and olivine/sand treatments is higher compared to grain-collision batch experiments (Flipkens et al., 2023; England and Bach, 2025).

4.3. The absent *additionality problem*

In mixed olivine and sand batch experiments, Bach (2024) identified a decline in natural TA release from the dissolution of carbonate minerals contained in sand when adding olivine: this was defined as the *additionality problem*. Natural sands can contain carbonate (here up to 14 wt% (calcite, high Mg-calcite and aragonite; supplementary Table S4), and when in contact with corrosive seawater or pore water, can dissolve causing a natural increase in TA (Middelburg et al., 2020; Torres et al., 2020). In our study, an indication for carbonate dissolution is only seen in changes in the CaO content of the sand, which decreased by ~1 wt.% in the turbulent sand treatments (supplementary Fig. S6b; Table S4). However, in all our experimental treatments and in the seawater reference, carbonate minerals were oversaturated (Ω_{Ar} > 1; Fig. 4c), and should therefore not dissolve. The addition and subsequent dissolution of olivine even increased the carbonate saturation state to higher levels, further inhibiting the dissolution of sand-occurring carbonates.

Next to carbonates, feldspars are highly abundant in the used sand, making up to 30.4 wt.% (plagioclase and microcline; supplementary Table S4) and, as plagioclase contains Ca, could also be responsible for the Ca loss in the solids upon dissolution (supplementary Fig. S6b,c; Table S4). Though being highly reactive in seawater, dissolution rates of feldspars (plagioclase) are about 20% lower compared to olivine (forsterite) (Jeandel and Oelkers, 2015). Nevertheless, feldspars can dissolve quickly when initially in contact with seawater, having the potential to impact marine element cycling

https://doi.org/10.5194/egusphere-2026-3096
Preprint. Discussion started: 10 June 2026

(Geilert et al., 2023). While high seawater background concentrations of Na, K and Ca inhibit a direct correlation with mineral dissolution, a strong increase in Sr and Li concentrations is visible only in the sand-bearing treatments compared to sand-free experimental treatments (Fig. 5c, d). While Sr continuously increased over the experiment, Li showed a decrease after ca. T+100 h. This may indicate the precipitation of secondary minerals, however, this is not directly visible in the TA concentrations of the sand-bearing treatments (see section 4.2 and 4.4). Also, Sr is lost from the solids of sand and the olivine/sand treatments, which was most pronounced in the turbulent olivine/sand treatment (supplementary Figure S6e,f). Unfortunately, we cannot unequivocally identify the mineral source and later sink of these elements, as Sr and Li are both enriched in carbonates and feldspars (Bentley, 2006; Penniston-Dorland et al., 2017). In addition, the stoichiometric balances discern that the dissolution of carbonates and feldspars produce the same amount of TA (2 HCO_3^-); therefore, we cannot further constrain the TA source in the sand treatments based on our data set. Nevertheless, we can conclude, that TA generation in the sand treatments are lower, or equal, throughout the experiment compared to the olivine/sand treatments. Thus, the natural TA release by sand was not hampered by the addition of olivine. The reason for this might be the constant dilution with seawater in our flow-through experiments, which keeps TA accumulation below the critical thresholds, and thereby prevent mineral dissolution in the sand from carbonates or feldspars—as was observed in batch experiments by (Bach, 2024b). Therefore, extrapolating our results to OAE beach applications, we conclude that the *additionality problem* might occur less than originally proposed. Nevertheless, the mineralogical composition of beach sands is of crucial importance and the composition of naturally occurring alkaline minerals should be assessed before a universal conclusion for OAE implications can be drawn.

4.4. Minimal probability of secondary mineral precipitation

Assessing the probability of secondary mineral precipitation in the OAE context is essential as the formation of carbonates and phyllosilicates is a source of CO_2, which reduces the net CO_2-sequestration potential of a system (Griffioen, 2017; Rigopoulos et al., 2018; Fuhr et al., 2022; Hartmann et al., 2022; Moras et al., 2022). In our flow-through experiments, the constant dilution with seawater reduced the probability of secondary mineral formation, as mineral saturation states were less likely to be attained. In the turbulent treatments, TA was always higher compared to the incoming seawater reference, indicating that no significant TA loss was due to secondary mineral formation (Fig. 2 and 3). Only in the stagnant olivine/sand treatments, negative TA values (and fluxes) were observed, indicating the formation of secondary minerals, potentially as carbonates (see section 4.2), as phyllosilicates and $Fe(OH)_3$ were undersaturated throughout the experiment (supplementary Fig. S7).

Interesting was the sharp drop in Li after T+144h, which occurred in all treatments except for the olivine treatment and the incoming seawater reference (Fig. 5d). Li can be incorporated into carbonate and phyllosilicate minerals, however, saturation states for the phyllosilicates sepiolite and chrysotile, which can form in seawater under ambient conditions (Wimpenny et al., 2010; Griffioen, 2017; Rigopoulos et al., 2018), show oversaturation only in the first hours of the experiment (up to T+100h) and then decrease quickly to undersaturated values (supplementary Fig. S7). Therefore, phyllosilicate formation likely played a minor role in our experiments with respect to TA, though small increases in the solid concentrations of SiO_2 and MgO are present in the turbulent olivine/sand treatments (supplementary Fig. S6c). It is striking that the strong Li decrease only occurred in the sand-bearing treatments. This points to the formation of secondary Si-phases (Fig. 4e). We speculate, that the dissolution of feldspars in sand (30.4 wt.%; supplementary Fig. S3 and Table S4) releases Al, that induces Si-Al co-precipitation, as Al lowers the saturation state of Si-bearing phases (Van Cappellen and Qiu, 1997) without impacting TA. Secondary amorphous Si-Al phases often occur as a precursor

https://doi.org/10.5194/egusphere-2026-3096
Preprint. Discussion started: 10 June 2026

clay phase in marine sediments and could also form in our experiments when certain Si and Al concentrations are reached (Baldermann et al., 2013). This would also explain why Si was below detection limit after about T+100 h for most sand-bearing treatments (Fig. 4b). The formation of amorphous metal (Al)-SiO_2 precipitates could also explain why TA concentrations (Fig. 2e,f) and fluxes (Fig. 3) merged with the pure turbulent olivine treatment after circa T+144h. That is, by forming passivating surface layers on top of the olivine grains (Béarat et al., 2006; Oelkers et al., 2018), despite vigorous grain collision. If trace metals, such as Li, are taken up in these amorphous Si-Al phases still needs to be tested, but our data is a strong indication for this process.

4.5. Release of trace metals

The release of potentially toxic trace metals, such as Ni and Cr, is highest in all olivine-bearing turbulent treatments in the beginning of the experiment (Fig. 5a). The turbulent treatments show Ni concentrations about 20-times higher than incoming background seawater, whereas the turbulent olivine treatment showed 100-times higher Ni values (supplementary Table S3). These high Ni concentrations exceed the recommended EU guidelines for marine waters, which are 64 nmol for Ni L^{-1}, and a magnitude lower for Cr concentrations, with maximum values of 96 µmol Cr L^{-1} (Nickel institute 2012; Vaiopoulou and Gikas, 2020). Studies have shown that dissolved Ni concentrations above certain threshold values can affect several marine species (Bach et al., 2019; Guo et al., 2022; Flipkens et al., 2023, 2024; Pernet et al., 2026). Although, some studies have found neutral and positive effects of high Ni concentrations (Hutchins et al., 2023; Jankowska et al., 2026). The fast decline of Ni after T+24h to concentrations below the EU guideline values for the olivine/sand treatment limits the risk of potentially toxic exposure for the sensitive organisms in the water column. Interestingly, Ni shows an enrichment of 200 ppm in the solid phase after the experiment (supplementary Table S6). We speculate, that the potential formation of $Ni(OH)_2$ phases, like theophrastite, in the olivine/sand treatment could also provide a sink for Ni, given that the solubility of Ni species is extremely low under alkaline conditions (Mattigod et al., 1997). The uptake of potentially toxic trace metals in secondary metal hydroxides and phyllosilicates was also observed by Fuhr et al. (2022), and could limit the risk of attaining toxic levels of trace metals in the natural environment. With respect to potential field tests, the release of high levels of dissolved Ni and Cr should be avoided, like in the beginning of the experiment, in real-world applications. For example, an olivine deployment may be performed in subsequent phases, and not via a one-time application of large amounts. This would also be in favour with respect to the settling behaviour of marine gastropods, where an avoidance of olivine settlement was observed, when concentrations exceeded 30%w/w, in addition to ambient environmental controls (Flipkens et al., 2024).

4.6. OAE potential of beach applications

Our experiments show that grain collision is efficient and can enhance the natural TA generation on beaches. In the flow-through experimental setup used in this study, no hindrance of the natural TA release from mineral dissolution (carbonates and/or feldspars) was observed, as described in the batch experiments from Bach (2024). The high flow rate in our system provided a constant dilution with seawater, which is comparable to natural beach settings. This can likely keep the solution undersaturated (or supersaturated at low levels) with respect to these minerals.

The efficiency of olivine dissolution and, thus, TA generation has been shown in several laboratory experiments by now (Fuhr et al., 2022, 2024; Flipkens et al., 2023; Bach, 2024; Geerts et al., 2025;

https://doi.org/10.5194/egusphere-2026-3096
Preprint. Discussion started: 10 June 2026

England and Bach, 2025). However, transfer to field settings, and more specifically the detection and quantification of olivine-generated TA in contrast to natural alkalinity release remains challenging (Fuhr et al., 2023; Geerts et al., 2025; Kreuzburg et al., 2025). The next crucial step with respect to OAE is a reliable method of monitoring, reporting and verification (MRV). Tracer development is required and a potential strategy might be the use of stable isotope systems of silicon (Si) or nickel (Ni) (Geerts et al., 2025). With respect to our experiments, the use of stable Si isotopes was hindered due to low Si concentrations (below detection limit) resulting from high dilution rates with ambient seawater, which is also a likely scenario in field settings. Nickel, in contrast, remains at detectable concentrations throughout the experiment and could therefore be a suitable candidate for stable isotope applications and tracer development.

With respect to beach OAE applications, next to natural TA release, the transport, deposition and burial of the olivine grains out of the high-energy environment in the surf zone impose additional challenges. However, as much as this is considered a challenge in beach applications, this process could also offer another route for TA generation via macrofauna bioturbation, digestion and microbial processes (Meysman and Montserrat, 2017; Eisaman et al., 2023). Recent studies show, that microbial processes in the benthic environment are quite efficient in enhancing mineral dissolution, though in the case of the Baltic Sea, carbonate dissolution was identified to dominate over olivine dissolution (Fuhr et al., 2023, 2024, 2025; Dale et al., 2024). If the transport and burial of olivine along the shelf has a similar effect, this needs to be investigated, but could provide an additional alkalinity source next to the alkalinity generated in the surf zone. In addition, olivine deployment would be facilitated by this natural transport process, as olivine spreading at beaches is more feasible compared to shelf deployments via the logistics involved in using marine vessels (Foteinis et al., 2023).

Conclusion

Ocean alkalinity enhancement in coastal environments is considered an efficient and low-cost technique in the context of CO_2-removal as climate change mitigation strategy. In this study, we simulated the addition of olivine to beaches in a turbulent flow-through reactor experiment, in which grain collision was hypothesized to increase mineral dissolution. Our experiments show efficient mineral grinding under turbulent conditions and alkalinity generation up to 2-times higher compared to stagnant conditions, and up to 9-times higher during high mineral reaction rates at the beginning of the experiment. Our alkalinity increases are 2.5-times higher compared to grain collision experiments in batch reactors. Thus, our experiments show an argument for an additional mineral dissolution effect under olivine-undersaturated conditions due to the constant flushing with seawater, which resembles natural field conditions more closely. Our experiments also show, that under high fluid-exchange rates, a decline in natural alkalinity (i.e, by carbonate mineral dissolution in the natural sand) is negligible, as critical mineral saturation levels can be avoided. Potential toxic trace metal release was observed to be highest in the first hours of the experiment when mineral reaction rates were fast. With experimental time, Ni concentrations decreased to values below critical concentration guidelines, likely lowering the risk of negatively impacting the pelagic marine ecosystem. The avoidance of these critical concentration overshoots should be one of the main foci when extrapolating to field applications to keep OAE a viable method to mitigate climate change.

https://doi.org/10.5194/egusphere-2026-3096
Preprint. Discussion started: 10 June 2026

Author contribution

SG and CAM conceptualized the study and designed the experimental setup. LH and JV conducted the experiments and determined seawater properties. FP provided the experimental facilities and supervised the experiments. AB and YBHA conducted the solid sample analyses and interpreted the results. JV supported during the fluid analyses. SG wrote the manuscript and all authors contributed to interpretation and provided feedback.

Competing interests

The contact author has declared that none of the authors has any competing interest

Acknowledgements

The authors thank the research technicians at Sité Experimental d'Argenton (Ifremer) and the technicians at the GeoLab (Utrecht University) for their support during the experiment and subsequent analyses.

Financial support

This study was funded from the Prince Albert II of Monaco Foundation (Project: REPAIRS: finance agreementN°4000.2-1).

Data availability

All data are included within the article and the supplement (supplementary figures and tables).

References

Bach L. T. (2024) The additionality problem of ocean alkalinity enhancement. *Biogeosciences* **21**, 261–277.

Bach L. T., Gill S. J., Rickaby R. E. M., Gore S. and Renforth P. (2019) CO2 Removal With Enhanced Weathering and Ocean Alkalinity Enhancement: Potential Risks and Co-benefits for Marine Pelagic Ecosystems. *Frontiers in Climate* **1**.

Baldermann A., Warr L. N., Grathoff G. H. and Dietzel M. (2013) The rate and mechanism of deep-sea glauconite formation at the Ivory Coast - Ghana Marginal Ridge. *Clays Clay Miner.* **61**, 258–276.

Béarat H., McKelvy M. J., Chizmeshya A. V. G., Gormley D., Nunez R., Carpenter R. W., Squires K. and Wolf G. H. (2006) Carbon Sequestration via Aqueous Olivine Mineral Carbonation: Role of Passivating Layer Formation. *Environ. Sci. Technol.* **40**, 4802–4808.

Bentley R. A. (2006) Strontium isotopes from the earth to the archaeological skeleton: A review. *J. Archaeol. Method Theory* **13**, 135–187.

https://doi.org/10.5194/egusphere-2026-3096
Preprint. Discussion started: 10 June 2026

788 Van Cappellen P. and Qiu L. Q. (1997) Biogenic silica dissolution in sediments of the Southern
789 Ocean.1. Solubility. *Deep-Sea Research Part Ii-Topical Studies in Oceanography* **44**, 1109–1128.

790 Dale A. W., Geilert S., Diercks I., Fuhr M., Perner M., Scholz F. and Wallmann K. (2024) Seafloor
791 alkalinity enhancement as a carbon dioxide removal strategy in the Baltic Sea. *Commun. Earth*
792 *Environ.* **5**.

793 Eisaman M., Geilert S., Renforth P., Bastianini L., Campbell J., Dale A. W., Foteinis S., Grasse P., Hawrot
794 O., Löscher C., Rau G. and Ronning J. (2023) Assessing technical aspects of ocean alkalinity
795 enhancement approaches. *State of the Planet Discussions*, 1–52.

796 England P.I. and Bach L. T. (2025) Influence of Wave Action on Applications of Olivine - Based Ocean
797 Alkalinity Enhancement on Sandy Beaches. *Geophys. Res. Lett.* **53**, 1–10.

798 Flipkens G., Dujardin V., Salden J., T'Jollyn K., Town R. M. and Blust R. (2024) Olivine avoidance
799 behaviour by marine gastropods (Littorina littorea L.) and amphipods (Gammarus locusta L.)
800 within the context of ocean alkalinity enhancement. *Ecotoxicol. Environ. Saf.* **270**.

801 Flipkens G., Fuhr M., Fiers G., Meysman F. J. R., Town R. M. and Blust R. (2023) Enhanced olivine
802 dissolution in seawater through continuous grain collisions. *Geochim. Cosmochim. Acta* **359**,
803 84–99.

804 Foteinis S., Campbell J. S. and Renforth P. (2023) Life Cycle Assessment of Coastal Enhanced
805 Weathering for Carbon Dioxide Removal from Air. *Environ. Sci. Technol.* **57**, 6169–6178.

806 Friedlingstein P., O'Sullivan M., Jones M. W., Andrew R. M., Hauck J., Landschützer P., Le Quéré C., Li
807 H., Luijkx I. T., Olsen A., Peters G. P., Peters W., Pongratz J., Schwingshackl C., Sitch S., Canadell J.
808 G., Ciais P., Jackson R. B., Alin S. R., Arneth A., Arora V., Bates N. R., Becker M., Bellouin N.,
809 Berghoff C. F., Bittig H. C., Bopp L., Cadule P., Campbell K., Chamberlain M. A., Chandra N.,
810 Chevallier F., Chini L. P., Colligan T., Decayeux J., Djeutchouang L. M., Dou X., Duran Rojas C.,
811 Enyo K., Evans W., Fay A. R., Feely R. A., Ford D. J., Foster A., Gasser T., Gehlen M., Gkritzalis T.,
812 Grassi G., Gregor L., Gruber N., Gürses Ö., Harris I., Hefner M., Heinke J., Hurtt G. C., Iida Y.,
813 Ilyina T., Jacobson A. R., Jain A. K., Jarníková T., Jersild A., Jiang F., Jin Z., Kato E., Keeling R. F.,
814 Klein Goldewijk K., Knauer J., Korsbakken J. I., Lan X., Lauvset S. K., Lefèvre N., Liu Z., Liu J., Ma
815 L., Maksyutov S., Marland G., Mayot N., McGuire P. C., Metzl N., Monacci N. M., Morgan E. J.,
816 Nakaoka S.-I., Neill C., Niwa Y., Nützel T., Olivier L., Ono T., Palmer P. I., Pierrot D., Qin Z.,
817 Resplandy L., Roobaert A., Rosan T. M., Rödenbeck C., Schwinger J., Smallman T. L., Smith S. M.,
818 Sospedra-Alfonso R., Steinhoff T., Sun Q., Sutton A. J., Séférian R., Takao S., Tatebe H., Tian H.,
819 Tilbrook B., Torres O., Tourigny E., Tsujino H., Tubiello F., van der Werf G., Wanninkhof R., Wang
820 X., Yang D., Yang X., Yu Z., Yuan W., Yue X., Zaehle S., Zeng N. and Zeng J. (2025) Global Carbon
821 Budget 2024. *Earth Syst. Sci. Data* **17**, 965–1039.

822 Fuhr M., Dale A. W., Wallmann K., Bährle R., Kalapurakkal H. T., Sommer S., Spiegel T., Dobashi R.,
823 Buchholz B. and Geilert S. (2025) Calcite is an efficient and low-cost material to enhance
824 benthic weathering in shelf sediments of the Baltic Sea. *Commun. Earth Environ.* **6**, 1–11.

825 Fuhr M., Geilert S., Schmidt M., Liebetrau V., Vogt C., Ledwig B. and Wallmann K. (2022) Kinetics of
826 Olivine Weathering in Seawater: An Experimental Study. *Frontiers in Climate* **4**, 1–20.

827 Fuhr M., Wallmann K., Dale A. W., Diercks I., Kalapurakkal H. T., Schmidt M., Sommer S., Böhnke S.,
828 Perner M. and Geilert S. (2023) Disentangling artificial and natural benthic weathering in
829 organic rich Baltic Sea sediments. *Frontiers in Climate* **5**.

https://doi.org/10.5194/egusphere-2026-3096
Preprint. Discussion started: 10 June 2026

Fuhr M., Wallmann K., Dale A. W., Kalapurakkal H. T., Schmidt M., Sommer S., Deusner C., Spiegel T., Kowalski J. and Geilert S. (2024) Alkaline mineral addition to anoxic to hypoxic Baltic Sea sediments as a potentially efficient CO2-removal technique. *Frontiers in Climate* **6**.

Gac J. P., Marrec P., Cariou T., Grosstefan E., Macé É., Rimmelin-Maury P., Vernet M. and Bozec Y. (2021) Decadal Dynamics of the CO2 System and Associated Ocean Acidification in Coastal Ecosystems of the North East Atlantic Ocean. *Front. Mar. Sci.* **8**.

Geerts Luna J.J., Hylén A. and Meysman F. J. R. (2025) Review and syntheses: Ocean alkalinity enhancement and carbon dioxide removal through marine enhanced rock weathering using olivine. *Biogeosciences* **22**, 355–384.

Geilert S., Frick D. A., Garbe-Schönberg D., Scholz F., Sommer S., Grasse P., Vogt C. and Dale A. W. (2023) Coastal El Niño triggers rapid marine silicate alteration on the seafloor. *Nat. Commun.* **14**, 1–8.

Griffioen J. (2017) Enhanced weathering of olivine in seawater: The efficiency as revealed by thermodynamic scenario analysis. *Science of the Total Environment* **575**, 536–544.

Guo J. A., Strzepek R., Willis A., Ferderer A. and Bach L. T. (2022) Investigating the effect of nickel concentration on phytoplankton growth to assess potential side-effects of ocean alkalinity enhancement. *Biogeosciences* **19**, 3683–3697.

Hartmann J., Suitner N., Lim C., Schneider J., Marín-Samper L., Arístegui J., Renforth P., Taucher J. and Riebesell U. (2023) Stability of alkalinity in Ocean Alkalinity Enhancement (OAE) approaches - consequences for durability of CO2 storage. *Biogeosciences* 20, 781–802.

Hutchins D. A., Fu F. X., Yang S. C., John S. G., Romaniello S. J., Andrews M. G. and Walworth N. G. (2023) Responses of globally important phytoplankton species to olivine dissolution products and implications for carbon dioxide removal via ocean alkalinity enhancement. *Biogeosciences* **20**, 4669–4682.

IPCC, 2023: Climate Change 2023: Synthesis Report. Contribution of Working Groups I, II and III to the Sixth Assessment Report of the Intergovernmental Panel on Climate Change [Core Writing Team, H. Lee and J. Romero (eds.)], Geneva, Switzerland.

Jeandel C. and Oelkers E. H. (2015) The influence of terrigenous particulate material dissolution on ocean chemistry and global element cycles. *Chem. Geol.* **395**, 50–66.

Kreuzburg M., Hylén A., Cole D. B., Romaniello S. J., Winardhi C. W., Cnudde V., Frick D. A., Barnett J., Nicolaysen K. P. and Meysman F. J. R. (2025) Hawaiian beaches as natural analogues for enhanced silicate weathering of olivine. *Environmental Research Letters* **20**, 114074.

Lueker T. J., Dickson A. G. and Keeling C. D. (2000) Ocean pCO calculated from dissolved inorganic carbon, alkalinity, and equations for K1 and K2: validation based on laboratory measurements of CO2 in gas and seawater at equilibrium. *Mar. Chem.* **70**, 105–119.

Mendes I., Lübbers J., Schönfeld J., Baldermann A., Carrasco A. R., Cravo A., Gomes A., Grasse P. and Stamm F. M. (2025) Novel Field Experiment on Alkalinity Enhancement in Intertidal Environments—A Trailblazer for Natural Climate Solutions. *J. Geophys. Res. Biogeosci.* **130**.

Meysman F. J. R. and Montserrat F. (2017) Negative CO2 emissions via enhanced silicate weathering in coastal environments. *Biological Letters* **13**.

https://doi.org/10.5194/egusphere-2026-3096
Preprint. Discussion started: 10 June 2026

Middelburg J. J., Soetaert K. and Hagens M. (2020) Ocean alkalinity, buffering and biogeochemical processes. *Reviews of Geophysics* **58**.

Miller C. A. and Pernet F. (2025) The alkalinity generation potential of olivine and oyster shell for laboratory experiments: testing the effects of ocean alkalinity enhancement. *Environ. Res. Commun.* **7**.

Montserrat F., Renforth P., Hartmann J., Leermakers M., Knops P. and Meysman F. J. R. (2017) Olivine Dissolution in Seawater: Implications for CO2 Sequestration through Enhanced Weathering in Coastal Environments. *Environ. Sci. Technol.* **51**, 3960–3972.

Moras C. A., Bach L. T., Cyronak T., Joannes-Boyau R. and Schulz K. G. (2022) Ocean alkalinity enhancement - avoiding runaway CaCO3 precipitation during quick and hydrated lime dissolution. *Biogeosciences* **19**, 3537–3557.

Nickel Institute 2012. Data compilation, selection and derivation of PNEC values for the marine aquatic environment. European Union Environmental Risk Assessment on Nickel. Available from: https://ec.europa.eu/health/ph_risk/committees/04_scher/docs/scher_o_112.pdf.

Oelkers E. H., Declercq J., Saldi G. D., Gislason S. R. and Schott J. (2018) Olivine dissolution rates : A critical review. *Chem. Geol.* **500**, 1–19.

Oschlies A., Bach L. T., Rickaby R. E. M., Satterfield T., Webb R. and Gattuso J. -P. (2023) Climate targets, carbon dioxide removal, and the potential role of ocean alkalinity enhancement. *State of the Planet*, 1–9.

Parkhurst D. L. and Appelo C. A. J. (2013) *Description of Input and Examples for PHREEQC Version 3 — A Computer Program for Speciation , Batch-Reaction , One-Dimensional Transport , and Inverse Geochemical Calculations*. book 6, ch., U.S. Geological Survey Techniques and Methods.

Penniston-Dorland S., Liu X.-M. and Rudnick R. L. (2017) Lithium Isotope Geochemistry. *Rev. Mineral. Geochem.* **82**, 165–217.

Pernet F., Ducoulombier L., Koechlin H., Gazeau F. and Miller C. A. (2026) Alkaline mineral dissolution can impair embryonic development in the Pacific oyster (Magallana gigas), raising caution for ocean alkalinity enhancement. *ICES Journal of Marine Science* **83**.

Pierrot D. E., Wallace D. W. R. and Lewis E. (2011) MS Excel Program Developed for CO2 System Calculations. *Carbon Dioxide Information Analysis Center*.

Richoz S., Baldermann A., Frauwallner A., Harzhauser M., Daxner-Höck G., Klammer D. and Piller W. E. (2017) Geochemistry and mineralogy of the Oligo-Miocene sediments of the Valley of Lakes, Mongolia. *Paleobiodivers. Paleoenviron.* **97**, 233–258.

Rigopoulos I., Harrison A. L., Delimitis A., Ioannou I., Efstathiou A. M., Kyratsi T. and Oelkers E. H. (2018) Carbon sequestration via enhanced weathering of peridotites and basalts in seawater. *Applied Geochemistry* **91**, 197–207.

Suitner N., Faucher G., Lim C., Schneider J., Moras C. A., Riebesell U. and Hartmann J. (2024) Ocean alkalinity enhancement approaches and the predictability of runaway precipitation processes: results of an experimental study to determine critical alkalinity ranges for safe and sustainable application scenarios. *Biogeosciences* **21**, 4587–4604.

https://doi.org/10.5194/egusphere-2026-3096
Preprint. Discussion started: 10 June 2026

909 Torres M. E., Hong W.-L., Solomon E. A., Milliken K., Kim J.-H., Sample J. C., Teichert B. M. A. and
910 Wallmann K. (2020) Silicate weathering in anoxic marine sediment as a requirement for
911 authigenic carbonate burial. *Earth. Sci. Rev.* **200**.

912 Vaiopoulou E. and Gikas P. (2020) Regulations for chromium emissions to the aquatic environment in
913 Europe and elsewhere. *Chemosphere* **254**, 126876.

914 Wimpenny J., Gíslason S. R., James R. H., Gannoun A., Pogge Von Strandmann P. A. E. and Burton K.
915 W. (2010) The behaviour of Li and Mg isotopes during primary phase dissolution and secondary
916 mineral formation in basalt. *Geochim. Cosmochim. Acta* **74**, 5259–5279.

917 Zeebe R. E. and Wolf-Gladrow D. (2006) *CO2 in Seawater: Equilibrium, Kinetics, Isotopes*. ed. David
918 Halpern, Elsevier Oceanography Series, Amsterdam.

919